Lateral Entry Guidance With Terminal Time Constraint

ZIXUAN LIANG
CHANG LV
SHENGYING ZHU
Beijing Institute of Technology, Beijing, China
Key Laboratory of Autonomous Navigation and Control for Deep Space Exploration, Ministry of Industry and Information Technology, Beijing, China

A simultaneous attack mission requires the entry vehicle to be capable of controlling the terminal time. To satisfy the terminal time constraint and meanwhile to cooperate with the previous longitudinal guidance algorithms, a lateral entry guidance method is developed using a closed-loop trajectory predictor for the terminal time, a bank reversal logic based on a double-corridor strategy, and a terminal time determination approach. The double-corridor contains a time error corridor used to activate the modification of the terminal time, and an adjustable heading corridor, when activated, used to reduce the terminal time error. The desired terminal time is calculated according to a feasibility index, which describes the tolerance of aerodynamic dispersions. The simulations of a time constrained entry flight show that the lateral guidance method can achieve a high accuracy of the terminal time control while satisfying the conventional entry constraints. The advantage of the desired terminal time given by the feasibility index is also demonstrated.

Manuscript received 28 February 2022; revised 19 September 2022; accepted 14 October 2022. Date of publication 19 October 2022; date of current version 9 June 2023.

DOI. No. 10.1109/TAES.2022.3215554

Refereeing of this contribution was handled by S. Le Menec.

This work was supported in part by the National Natural Science Foundation of China under Grant 61803008 and Grant 62073034, in part by the Basic Scientific Research Program of China under Grant JCKY2018602B002, and in part by the Space Debris Research Project of China under Grant KJSP2020020302.

Authors' address: The authors are with the School of Aerospace Engineering, Beijing Institute of Technology, Beijing 100081, China, and also with the Key Laboratory of Autonomous Navigation and Control for Deep Space Exploration, Ministry of Industry and Information Technology, Beijing 100081, China, E-mail: (liangzx@bit.edu.cn; sxfylc@163.com; zhushy@bit.edu.cn). *(Corresponding author: Zixuan Liang.)*

I. INTRODUCTION

With the aid of aerodynamic forces, an entry vehicle is able to perform a gliding trajectory in the near-space and complete a global attack. The success of an entry flight is guaranteed by an advanced guidance system. During the past decades, excellent works have been done for the entry guidance to improve the accuracy, reliability, and adaptivity [1], [2], [3], [4], [5], [6]. To date, the essential requirements for traditional landing guidance are almost fulfilled, which is also indicated by the successful flight of some entry vehicles [7]. In such case, more and more attentions are paid to the penetration capability of target reconnaissance [8], [9], threat avoidance [10], [11], and cooperative attack [12], [13].

A cooperative attack mission requires multiple entry vehicles to cooperate in time (e.g., reach the terminal zone simultaneously) or space (e.g., reach the terminal zone from various directions [14]). To achieve a simultaneous attack, the entry vehicle is required to be capable of controlling the terminal time. As remote communication among multiple entry vehicles is too difficult to achieve, each vehicle is expected to fly independently and reach the terminal zone at a preset time. Thus, the terminal time constraint becomes necessary to be considered on the basis of conventional constraints. The conventional entry constraints refer to path constraints (e.g., heating rate, aerodynamic load, and dynamic pressure) and terminal condition constraints (e.g., altitude, velocity, and range-to-go). The terminal time constraint, which is ignored in previous works, would make the design of entry guidance more challenging.

The terminal time constrained guidance, also known as the impact time control guidance, has been addressed for missiles in the homing phase [15], [16], [17], [18], [19], [20]. In [15], [16], [17], and [18], the guidance command is designed by the combination of a proportional navigation guidance part and a feedback part of the impact time. In [19] and [20], the impact time is achieved by tracking a desired time-to-go variable using the sliding mode control. These approaches, although performs well in the impact time control, are not applicable to entry vehicles due to the following reasons. First, the nonlinear forms such as the lift and drag cannot be ignored for the entry dynamics. Second, the assumption of the constant speed is invalid for entry vehicles without propulsive force. Third, the velocity heading angle is hard to be accurately controlled for entry vehicles which use a bank-to-turn mode. In [21], an impact time control method using a numerical time-to-go prediction is developed for a hypersonic vehicle. This method, although performs well in the terminal phase, is not applicable to the entry phase with multiple path constraints. Another issue for the cooperative attack is the determination of the desired terminal time. The terminal time for missiles only has a lower boundary, which relates to the initial range-to-go and the constant velocity [16], [17], [19]. In contrast, the terminal time for entry vehicles without propulsive force must take the upper boundary into account.

An ideal approach for the terminal time constraint of entry vehicles should be developed under the frame of typical entry guidance methods, which consist of a longitudinal guidance algorithm and a lateral guidance logic. In [12], a trajectory planning is proposed for the cooperative flight of two entry vehicles. The terminal time, which relates to the vehicle's lateral maneuver, is considered in the lateral guidance logic. Results show that the heading error corridor is able to control the terminal time error as well. In [22] and [23], the terminal time is handled by the longitudinal profile planning. However, the highly constrained longitudinal profile of an entry vehicle is undesirable to be frequently modified onboard, and moreover, the real-time performance of the planning algorithm cannot be guaranteed. In [24], an analytical solution using the quasi-equilibrium glide condition is proposed to estimate the terminal time, and the bank angle is modified to eliminate the time error. As modifications of the bank angle affect the longitudinal profile, the control of the terminal time would result in a large terminal velocity error. Therefore, the terminal time constraint is more suitable to be considered in the lateral guidance logic than the longitudinal guidance algorithm.

In this article, the terminal time constraint is considered together with the heading error constraint, and a lateral entry guidance logic based on double-corridor is developed. The inner one, a time error corridor, is used to activate the modification of the outer one, an adjustable heading error corridor, which is used to eliminate the predicted terminal time error. The adjustable heading error corridor is designed using a fractional-order function with a single adjustable parameter. The corridor can limit the heading error, and meanwhile, adjust to eliminate the terminal time error given by a closed-loop predictor. The determination of the desired terminal time is also investigated. In contrast to [12] that uses the average value of the minimum and maximum feasible time, we configure the desired time according to an index, which represents the feasibility of the terminal time under dispersions. The proposed guidance method is verified by numerical simulations, and the performance of the configured desired time is assessed by comparisons. The main contributions of this article are summarized as follows:

1) A novel lateral guidance method is developed under the typical entry guidance frame to control the entry terminal time. Compared with the previous approaches [22], [23], [24], the lateral guidance method has an advantage in cooperating with most of the previous longitudinal entry guidance algorithms [1], [6], [25], [26], [27], [28].
2) The proposed lateral guidance logic using a double-corridor can control both the heading error and the time error, while the previous lateral guidance logic only considers the heading error (or crossrange) [1], [27], [29]. Moreover, the double-corridor uses a low update rate for onboard modification, which ensures a good computational performance.
3) A novel method is proposed for the determination of desired terminal time. Compared with the average value of the minimum and maximum feasible time [12], the terminal time given by the feasibility index is more achievable for entry flights with uncertainties.

The rest of this article is organized as follows. In Section II, the entry guidance problem is formulated. In Section III, the lateral entry guidance method with the terminal time constraint is developed. Section IV verifies the effectiveness of the guidance method and the advantage of the terminal time determination approach. Finally, Section V concludes this article.

II. ENTRY GUIDANCE PROBLEM

A. Dynamics

With time as the independent variable, the three-dimensional point-mass dynamics of an entry vehicle over a rotating spherical earth are [30]

$$\frac{\mathrm{d}r}{\mathrm{d}t} = v\sin\gamma \tag{1}$$

$$\frac{\mathrm{d}v}{\mathrm{d}t} = -\frac{D}{m} - g\sin\gamma + \omega^2 r\cos\phi\big(\sin\gamma\cos\phi - \cos\gamma\sin\phi\cos\psi\big) \tag{2}$$

$$\frac{\mathrm{d}\gamma}{\mathrm{d}t} = \frac{1}{v}\left[\frac{L\cos\sigma}{m} - g\cos\gamma + \frac{v^2\cos\gamma}{r} + 2\omega v\cos\phi\sin\psi + \omega^2 r\cos\phi(\cos\gamma\cos\phi + \sin\gamma\sin\phi\cos\psi)\right] \tag{3}$$

$$\frac{\mathrm{d}\theta}{\mathrm{d}t} = \frac{v\cos\gamma\sin\psi}{r\cos\phi} \tag{4}$$

$$\frac{\mathrm{d}\phi}{\mathrm{d}t} = \frac{v\cos\gamma\cos\psi}{r} \tag{5}$$

$$\frac{\mathrm{d}\psi}{\mathrm{d}t} = \frac{1}{v}\left[\frac{L\sin\sigma}{m\cos\gamma} + \frac{v^2\cos\gamma\sin\psi\tan\phi}{r} - 2\omega v(\tan\gamma\cos\phi\cos\psi - \sin\phi) + \frac{\omega^2 r}{\cos\gamma}\sin\phi\cos\phi\sin\psi\right] \tag{6}$$

where t is the flight time, r is the radial distance from the Earth center to the vehicle, v is the velocity magnitude, γ is the flight-path angle, θ is the longitude, ϕ is the latitude, ψ is the velocity heading angle, σ is the bank angle, ω is the earth self-rotation rate, m is the vehicle mass, and g is the gravitational acceleration. The lift force L and drag force D are given by

$$\begin{cases} L = \frac{1}{2}\rho v^2 S_A C_L \\ D = \frac{1}{2}\rho v^2 S_A C_D \end{cases} \tag{7}$$

where ρ is the atmospheric density, S_A is the reference area, C_L is the lift coefficient, and C_D is the drag coefficient.

B. Constraints

During the entry flight, the typical path constraints are

$$\begin{cases} Q = K_Q \rho^{0.5} v^{3.15} \le Q_{\max} \\ n = \frac{\sqrt{L^2+D^2}}{m} \le n_{\max} \\ \bar{q} = 0.5\rho v^2 \le \bar{q}_{\max} \end{cases} \tag{8}$$

where $Q_{\max}$ is the maximum heating rate, $n_{\max}$ is the maximum aerodynamic load, $\bar{q}_{\max}$ is the maximum dynamic pressure, and K_Q is a constant.

The entry phase ends at the terminal interface with the range-to-go trigger. Let s_f be the radius of the terminal zone, i.e., the desired range-to-go. The terminal constraints are [10]

$$v(s_f) = v_f \tag{9}$$

$$h(s_f) = h_f \tag{10}$$

$$\left|\Delta\psi(s_f)\right| \le \Delta\psi_f \tag{11}$$

where h_f and v_f are the desired terminal altitude and velocity, respectively. The heading error $\Delta\psi$ is defined as the error between the heading angle and the line-of-sight angle toward the target, and $\Delta\psi_f$ is the allowable value at the terminal interface. The range-to-go from the vehicle to the target is computed using the great-circle distance

$$s = R_{\mathrm{E}} \arccos\left[\cos\phi\cos\phi_T\cos(\theta-\theta_T) + \sin\phi\sin\phi_T\right] \tag{12}$$

where the constant R_E is the radius of the earth, and θ_T and ϕ_T are the longitude and latitude of the target, respectively.

In addition to the traditional terminal constraints, the terminal time constraint is expressed as

$$t(s_f) = t_f \tag{13}$$

where t_f is the desired terminal time.

III. LATERAL ENTRY GUIDANCE METHOD

A. Guidance Strategy

The entry vehicle needs to be delivered to the terminal zone with the constraints in (8)–(11) and (13) satisfied. The path constraint in (8) can be considered in the longitudinal profile planning before the entry starts. Then, during the entry flight, (9) and (10) can be handled by a tracking law for the longitudinal profile which satisfies (8), and (11) can be handled by the lateral guidance logic using a heading error corridor [1]. Then, the main issue is the time constraint in (13).

The differential equation for the range-to-go is given by [31]

$$\frac{\mathrm{d}s}{\mathrm{d}t} = -\frac{vR_0\cos\gamma\cos\Delta\psi}{r}. \tag{14}$$

With the range-to-go as the independent variable, we have

$$\frac{\mathrm{d}t}{\mathrm{d}s} = -\frac{r}{vR_0\cos\gamma\cos\Delta\psi}. \tag{15}$$

Integrating (15) yields

$$t = t_0 + \frac{1}{R_0}\int_s^{s_0} \frac{r}{v\cos\gamma\cos\Delta\psi}\mathrm{d}s. \tag{16}$$

In (16), r, v, and γ belong to the longitudinal state, which would follow a reference profile under a tracking law. In such case, the flight time mainly relates to the heading error $\Delta\psi$. Therefore, the terminal time can be considered together with the heading angle in the lateral guidance logic and handled by the heading error corridor. Then, the guidance strategy is using a tracking law for the predesigned longitudinal profile, and an adjustable heading error corridor for the lateral guidance. In this article, the classical linear quadratic regulator is used as the tracking law, which is given by [10], [31]

$$\Delta\boldsymbol{u} = \boldsymbol{K}(s)\Delta\boldsymbol{X} \tag{17}$$

where $\Delta\boldsymbol{u} = [\Delta\sigma,\ \Delta\alpha]^{\mathrm{T}}$ is the adjustment of the bank angle and the angle of attack, and $\Delta\boldsymbol{X} = [\Delta r,\ \Delta v,\ \Delta\gamma]^{\mathrm{T}}$ is the tracking error of the longitudinal states. The feedback matrix $\boldsymbol{K}(s)$ is solved offline based on the Algebraic Riccati equation, and scheduled onboard with respect to the range-to-go s [31]. With the reference profiles and modifications, the guidance commands are

$$\begin{cases} \alpha = \alpha_{\mathrm{ref}} + \Delta\alpha \\ \sigma = (|\sigma_{\mathrm{ref}}| + \Delta\sigma)\mathrm{sgn}\sigma \end{cases} \tag{18}$$

where α_{ref} and σ_{ref} are the reference guidance commands corresponding to the longitudinal profile, and sgn σ is the sign of the bank angle given by the lateral guidance logic.

B. Closed-Loop Predictor for Terminal Time

Given the control variables, the entry trajectory can be predicted by numerically integrating the flight dynamics. The integration stops at the terminal interface according to the range-to-go. Then, the predicted terminal time is obtained, which is expressed as

$$t_p = P\left(\mathbf{Y}, f(\mathbf{Y}), \mathbf{u}, s_f\right) \tag{19}$$

where $\boldsymbol{Y} = [r,\ v,\ \gamma,\ \theta,\ \phi,\ \psi]^{\mathrm{T}}$ is the flight states, $f(\boldsymbol{Y})$ is the flight dynamics given by (1)–(6), and $\boldsymbol{u} = [\sigma, \alpha]^{\mathrm{T}}$ is the bank angle and the angle of attack.

For the conventional predictor-corrector algorithms widely used for the longitudinal guidance, the predictor outputs the predicted terminal state corresponding to the current control profiles, while the corrector adjusts the control profiles according to the error between the predicted and desired terminal states (in most cases, only the bank profile is adjusted). The control profiles determined by the corrector are not modified during the trajectory integration, i.e., an open-loop predictor is used. In this article, to get an accurately predicted trajectory, the control profiles used by the trajectory predictor should be consistent with that used during the actual flight. Therefore, the control profiles need to be modified during the trajectory prediction, and a closed-loop predictor is required.

For the closed-loop predictor, the modification of the control profiles is similar to the tracking law in (17), which

is given by

$$\Delta \boldsymbol{u}_p = \boldsymbol{K}(s)\Delta \boldsymbol{X}_p \tag{20}$$

where $\Delta \boldsymbol{u}_p$ is the modification of the control variables (i.e., the bank angle and the angle of attack) during the trajectory prediction, $\Delta \boldsymbol{X}_p$ is the state error between the predicted and reference trajectories, and the feedback matrix $\boldsymbol{K}(s)$ is the same as that in (17). With the modification of the control variables, the terminal time given by the closed-loop predictor is

$$t_p = P\left(\boldsymbol{Y}, f(\boldsymbol{Y}), \boldsymbol{u}_{\text{ref}} + \Delta \boldsymbol{u}_p, s_f\right) \tag{21}$$

where $\boldsymbol{u}_{\text{ref}} = [\alpha_{\text{ref}}, \sigma_{\text{ref}}]$ is the reference control variable.

Note that to improve the accuracy of the predictor, the onboard estimation and correction method in [32] is employed in calculating the lift and drag accelerations.

C. Terminal Time Control Using Double-Corridor

To adjust the terminal time while avoiding frequent bank reversals, a lateral guidance logic based on a double corridor strategy is employed. The double-corridor contains an inner corridor for time error and an outer corridor for heading error. The inner corridor is used to activate the modification of the outer corridor, which is used to eliminate the predicted terminal time error. For simplification, the inner corridor uses a constant time error boundary with the width denoted by B_1. Let t_p be the predicted terminal time, and Δt_p be the error between the predicted terminal time and the desired one. The output of the inner corridor is

$$M_{\text{on}} = \begin{cases} 0, & \left|\Delta t_p\right| \le B_1 \\ 1, & \left|\Delta t_p\right| > B_1 \end{cases} \tag{22}$$

where $M_{\text{ON}} = 1$ means that the modification of the outer corridor is activated in the current guidance cycle, while $M_{\text{on}} = 0$ indicates that the outer corridor remains unchanged.

The bank reversal logic under the outer corridor (i.e., the heading error corridor) is

$$\text{sgn}\sigma = \begin{cases} -1, & \text{if} \quad \Delta\psi > B_2(v) \\ \text{sgn}(\sigma_p), & \text{if} \quad |\Delta\psi| \le B_2(v) \\ 1, & \text{if} \quad \Delta\psi < -B_2(v) \end{cases} \tag{23}$$

where σ_p is the bank angle command in the previous guidance cycle, and $B_2(v)$ is the corridor boundary. The corridor in previous work [1], [27] is designed using a piecewise linear function of the velocity. The piecewise corridor is discrete and unsmooth, and thus is unsuitable to be adjusted onboard. To get a smooth heading error corridor, and meanwhile reduce the number of parameters, a fractional-order function is employed. The corridor boundary is expressed as

$$B_2(v) = B_f + k(v - v_1)^{1/4} - k\left(v_f - v_1\right)^{1/4} \tag{24}$$

where $k \ge 0$ is a width factor, v_1 is a specific velocity lower than the terminal velocity v_f, and B_f is the corridor boundary value at v_f. To satisfy the constraint in (11), we use

$$B_f = \eta \Delta\psi_f \tag{25}$$

where $0 < \eta < 1$ is a predesigned parameter. Then, for each value of k, the corridor boundary decreases with the velocity and close up at a velocity lower than v_f. Given v_1 and η, the unique adjustable variable of the corridor is the width factor. A larger width factor corresponds to a wider corridor, which would result in larger heading errors. Thus, according to (16), the width factor can be utilized for the terminal time control.

In (22), for the case $M_{\text{ON}} = 1$, the width factor needs to be adjusted to reduce the time error. Note that at different velocity, the adjustment of the width factor would produce different deviation of the corridor width. Thus, instead of the width factor, the corridor width given by (24) is chosen as the parameter to be adjusted. Let $k^{(1)}$ be the width factor given by the previous modification cycle, $b^{(1)}$ be the corresponding corridor width at the current velocity v, $\Delta t_p^{(1)}$ be the predicted terminal time error, and $\Delta\psi_p^{(1)}$ be the predicted terminal heading error. Consider the case $|\Delta\psi_p^{(1)}| \le \Delta\psi_f$. The adjustment of corridor width only needs to meet the terminal time requirement. To reduce the computational cost, the adjustment is given by

$$b = b^{(2)} - \frac{b^{(2)} - b^{(1)}}{\Delta t_p^{(2)} - \Delta t_p^{(1)}} \Delta t_p^{(2)} \tag{26}$$

where $\Delta t_p^{(2)}$ corresponds to $b^{(2)}$, which is set according to the sign of $\Delta t_p^{(1)}$

$$b^{(2)} = \begin{cases} b^{(1)} + \delta, & \text{if}\, \Delta t_p^{(1)} < 0 \\ b^{(1)} - \delta, & \text{if}\, \Delta t_p^{(1)} > 0 \end{cases} \tag{27}$$

where δ is a small positive value.

In the case $|\Delta\psi_p^{(1)}| \ge \Delta\psi_f$ (or $|\Delta\psi_p^{(2)}| \ge \Delta\psi_f$), the lateral trajectory is out of control, which indicates that the corridor is too wide. In such case, a smaller width is required, and the adjustment is simply given by

$$b = b^{(1)} - \delta. \tag{28}$$

Then, the width factor is

$$k = \frac{b - B_f}{(v - v_1)^{1/4} - \left(v_f - v_1\right)^{1/4}}. \tag{29}$$

Given the width factor, the heading error corridor is updated and used for the lateral guidance logic to determine the sign of the bank angle. Unlike the bank angle in conventional predictor-corrector algorithms, the heading error corridor affects the entry trajectory only when the heading error reaches the corridor boundary. Thus, the adjustment of the width factor is allowed to be completed in several modification cycles. In each cycle, the modification of the terminal time requires at most two numerically predicted trajectories, which means that the guidance method would not be time-consuming.

Note that the lateral guidance logic based on the heading error corridor works in each guidance cycle together with the longitudinal tracking law, while the adjustment of the corridor works only in the modification cycle for the terminal time. A wider modification cycle can further reduce the computational cost.

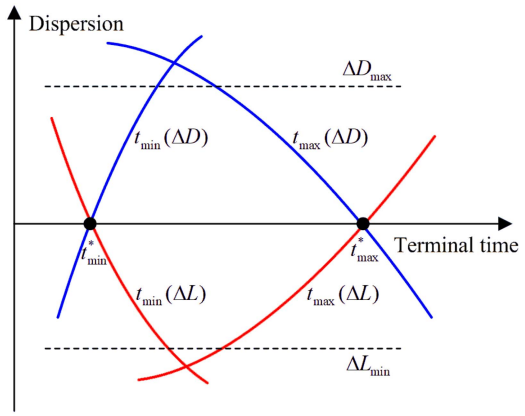

Fig. 1. Minimum and maximum terminal time under lift and drag dispersions.

D. Desired Terminal Time Determination

Unlike the terminal altitude and velocity, the terminal time is a relative index with respect to the initial time of the entry flight. Given the initial time, there exists a feasible interval of the terminal time. As the terminal time increases with the width factor, the minimum and maximum values are calculated by

$$\begin{cases} t^*_{\min} = t_p\big|_{k=0} \\ t^*_{\max} = \max\left\{t_p : k > 0,\ \left|\Delta\psi(s_f)\right| \le \Delta\psi_f\right\} \end{cases} \tag{30}$$

where the minimum time $t^*_{\min}$ is obtained using the narrowest corridor with $k = 0$, while the maximum time $t^*_{\max}$ corresponding to a wider corridor and a stronger lateral maneuver should guarantee the satisfaction of the terminal heading constraint.

The minimum and maximum terminal time are both calculated without the consideration of the aerodynamic uncertainties. Therefore, in practice with aerodynamic uncertainties, the feasibility cannot be guaranteed for each value in the interval $[t^*_{\min}, t^*_{\max}]$. The desired terminal time is configured as the average value of $t^*_{\min}$ and $t^*_{\max}$ in [12]. However, the influence of the aerodynamic uncertainties on the terminal time may not be symmetrical, which implies that the average value may not be the best choice.

The main aerodynamic uncertainties are the lift dispersion (refers to uncertainties of the lift coefficient, the density, and the mass) and the drag dispersion (refers to uncertainties of the drag coefficient, the density, and the mass). Let ΔL be the lift dispersion with respect to the nominal value. The minimum and maximum terminal time under the lift dispersion are denoted by $t_{\min}(\Delta L)$ and $t_{\max}(\Delta L)$, respectively. Similarly, for the drag dispersion ΔD, the minimum and maximum terminal time are denoted by $t_{\min}(\Delta D)$ and $t_{\max}(\Delta D)$, respectively. The terminal time under the lift and drag dispersions is illustrated in Fig. 1. The minimum time, which is achieved by the narrowest corridor, increases with the drag dispersion and decreases with the lift dispersion. The maximum time relates to the vehicle's lift-to-drag ratio, and thus, increases with the lift dispersion and decreases with the drag dispersion.

Let $\Delta D_{\max}$ and $\Delta L_{\min}$ be the maximum drag error and the minimum lift error of the entry vehicle, respectively. According to Fig. 1, for any $t \in (t^*_{\min}, t^*_{\max})$, the tolerable dispersion is constrained by $t_{\min}(\Delta L)$, $t_{\max}(\Delta L)$, $t_{\min}(\Delta D)$, $t_{\max}(\Delta D)$, $\Delta D_{\max}$, and $\Delta L_{\min}$. Here, a dispersion is considered to be tolerable when the terminal errors (altitude error, velocity error, and heading error) under this dispersion are acceptable. Thus, there exists a dispersion interval where t is feasible for the terminal time. The width of the interval represents the tolerance level of the dispersion. Let $\Delta_{\min}(t)$ and $\Delta_{\max}(t)$ be the lower and upper boundaries of the tolerable dispersion in Fig. 1. A feasibility index for the terminal time can be defined as follows:

$$\lambda(t) = \Delta_{\max}(t) - \Delta_{\min}(t). \tag{31}$$

Then, the optimal terminal time is configured by

$$\begin{aligned} t_f = \ & \arg\min_t \left| t - \frac{t^*_{\min} + t^*_{\max}}{2} \right| \\ \text{s.t.}\ & \lambda(t) = \max\{\lambda(t)\}. \end{aligned} \tag{32}$$

Compared with the terminal time given by the average value of the minimum and maximum feasible time, the optimal terminal time takes the tolerance of aerodynamic dispersions into account.

Note that calculation of the minimum and maximum terminal time relates to the time adjustment approach based on the heading error corridor. Nevertheless, the feasibility index given by (31) is also applicable to other time constrained guidance problems.

IV. NUMERICAL RESULTS

A. Simulation Conditions

The verification of the proposed guidance method uses the CAV-H model, which achieves the maximum lift-to-drag ratio of 3.5 at Mach 10 with the angle of attack around 10° (see [33] for details). The vehicle's mass, the atmospheric density, and the aerodynamic coefficients are modeled by

$$\begin{cases} m = (1 + \Delta m)m^* \\ \rho = (1 + \Delta\rho)\rho^* \\ C_L = (1 + \Delta C_L)C^*_L \\ C_D = (1 + \Delta C_D)C^*_D \end{cases} \tag{33}$$

where Δm is the mass error, $\Delta\rho$ is the density error, ΔC_L is the lift coefficient error, and ΔC_D is the drag coefficient error. The nominal mass is $= 907.2$ kg, and the nominal density $\rho*$ is given by the 1976 U.S. Standard Atmospheric. The nominal lift coefficient C^*_L and drag coefficient C^*_D can be found in [33]. In the nominal case, we set $\Delta m = 0$, $\Delta\rho = 0$, $\Delta C_L = 0$, and $\Delta C_D = 0$. In each of the dispersed cases, $\Delta\rho$ uses a simple model in both biased and altitude dependent fashions [34], and other parameters are all assumed to be constants and take values from a zero-mean Gaussian distribution. The three-sigma values (i.e., three times the standard deviations) for Δm, ΔC_L, and ΔC_D are 3, 10, and 10%, respectively.

TABLE I
Initial Entry Condition

Parameter	Nominal	3-sigma
Time, s	0	3
Altitude, km	60	2
Velocity, m/s	6400	50
Flight-path angle, deg	0	0.3
Longitude, deg	0	2
Latitude, deg	0	2
Heading angle, deg	56	3

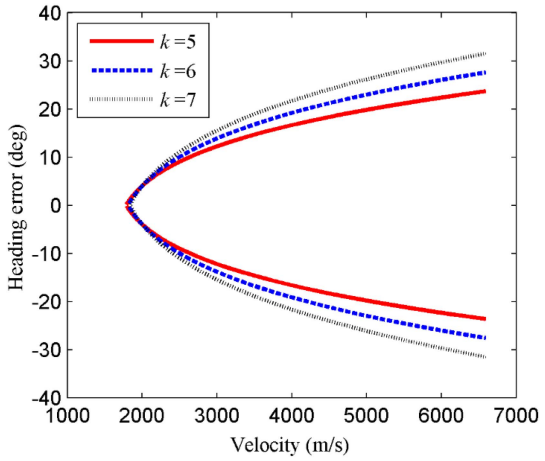

Fig. 2. Heading error corridor with various width factors.

The initial condition for the entry flight is shown in Table I. The terminal altitude and velocity are $h_f = 30$ km and $v_f = 2000$ m/s, respectively. The maximum allowable terminal heading error is $\Delta\psi_f = 5°$. The target's longitude and latitude are $\theta_T = 59°$ and $\phi_T = 30°$, respectively. The radius of the terminal zone is $s_f = 100$ km. The boundary of the time error corridor in (22) is $B_1 = 1$ s. The entry path constraints are $Q_{\max} = 4$ MW/m2, $n_{\max} = 3$ g, and $\bar{q}_{\max} = 60$ kPa. The guidance cycle update time is 1 s, and the corridor update time is 10 s. Parameters used for the heading error corridor are $v_1 = 1600$ m/s and $\eta = 0.8$. The fractional-order corridor with various width factors is illustrated in Fig. 2. For each value of k, the corridor boundary is found to decrease with the velocity and close up at a velocity lower than v_f.

B. Nominal Case

In the nominal case, the minimum and maximum terminal time is $t^*_{\min} = 1530$ s and $t^*_{\max} = 1694$ s, respectively. Set $\Delta D_{\max} = -\Delta L_{\min} = 25\%$. Then, the feasibility index for the terminal time is shown in Fig. 3. The maximum index is 0.5, which is achieved in the time interval [1541 s, 1584 s]. According to (32), the desired terminal time is 1584 s. With $t_f = 1584$ s as the terminal time constraint, the entry trajectory is flown using the proposed guidance method. Fig. 4(a) illustrates the altitude-velocity profile. The terminal altitude and velocity errors are 0.08 km and 2.07 m/s, respectively. Fig. 4(b) shows the ground track of the entry trajectory, which finally reaches the terminal zone. The heading error is shown in Fig. 4(c) together with the corridor (outer corridor). The fractional-order heading

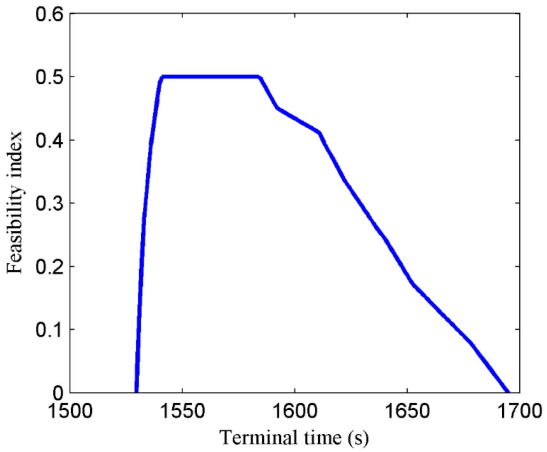

Fig. 3. Feasibility index of terminal time.

TABLE II
Terminal Errors in Dispersed Cases

Parameter	Mean	Standard deviation	Minimum	Maximum
Altitude error, km	0.08	0.17	-0.39	0.45
Velocity error, m/s	1.46	9.68	-23.28	24.83
Heading error, deg	-0.75	2.76	-4.73	4.77
Time error, s	0.09	0.57	-4.23	3.85

corridor is found to be effective in controlling the heading error whose terminal value is $-1.91°$. Since no dispersion is considered, the modification of the corridor is not performed during the flight. The corresponding guidance commands of the bank angle and the angle of attack are shown in Fig. 4(d). Four bank reversals are performed under the lateral guidance logic based on the double-corridor.

C. Dispersed Cases

The initial dispersions and aerodynamic uncertainties are considered using the Monte Carlo simulations with 500 runs. Fig. 5 shows the ground tracks that disperse widely during the flight but all reach the terminal zone. The heading errors are illustrated in Fig. 6. The corridors limit the heading error, and meanwhile, are adjusted to control the terminal time. The terminal errors of the proposed guidance method are shown in Table II. The standard deviations of the altitude and velocity are 0.17 km and 9.68 m/s, respectively. The terminal heading angle and time, which are controlled by the double-corridor, do not follow the Gaussian distribution. Nevertheless, the heading errors are within $\pm 5°$, and the time errors are within ± 5 s. Therefore, the proposed guidance method is demonstrated to be robust to entry dispersions.

The simulations in this article are conducted using MATLAB R2013b on a PC with 2 GHz CPU. The computation time (measured by the "tic-toc" function) taken by the guidance method in each cycle is recorded. The result for one of the 500 entry flights is illustrated in Fig. 7. A relatively high computation time is used for the trajectory prediction in every ten guidance cycles where the corridor update is required, especially for the cases where the outer corridor needs to be adjusted and the trajectories are predicted twice.

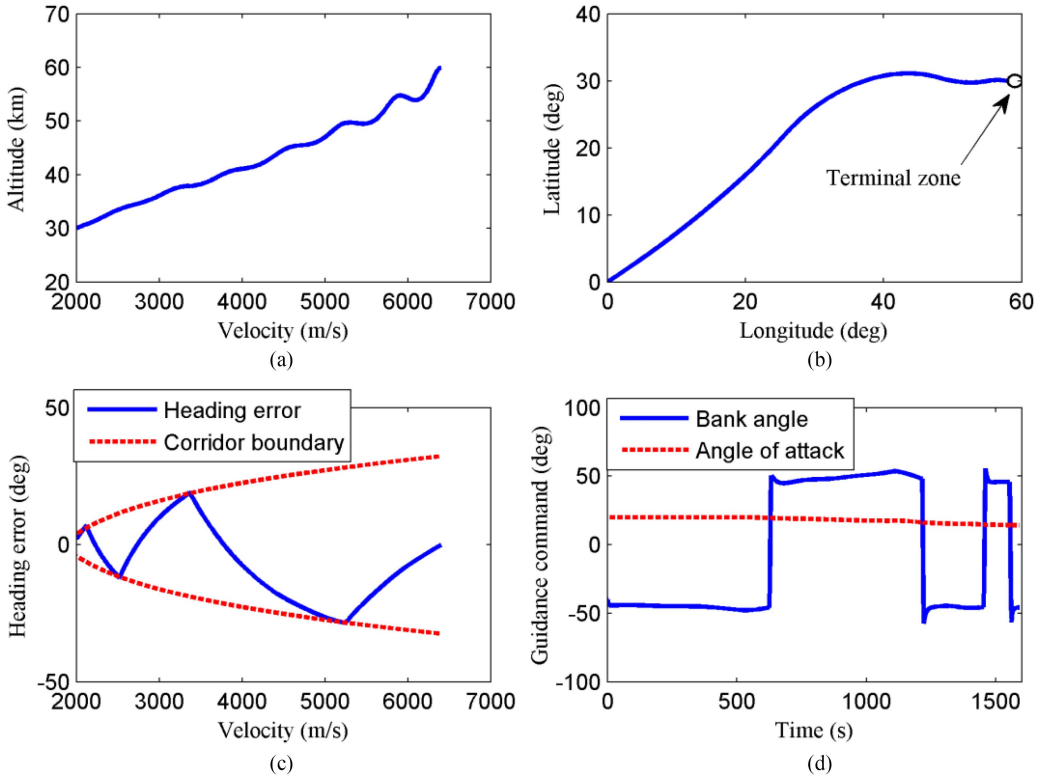

Fig. 4. Simulation results in nominal case. (a) Altitude-velocity. (b) Ground track. (c) Heading error. (d) Guidance command.

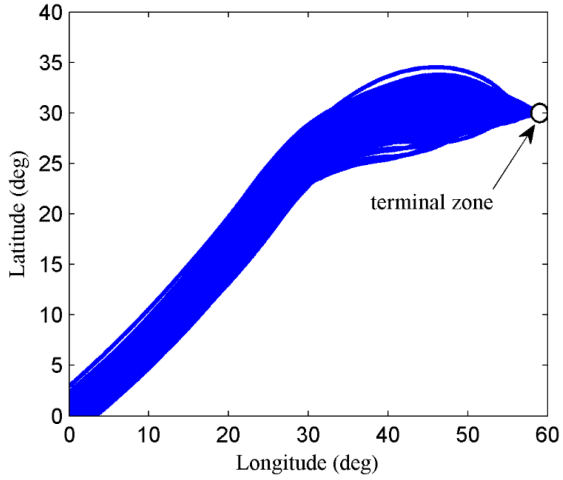

Fig. 5. Ground tracks in dispersed cases.

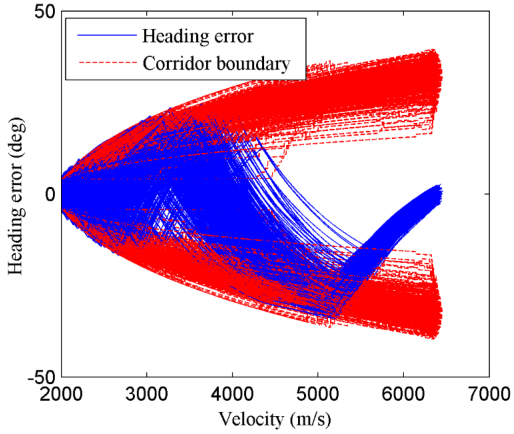

Fig. 6. Heading errors in dispersed cases.

The mean and maximum computation time for the guidance commands are only 0.02 s and 0.57 s, respectively. The result indicate that the proposed guidance method has a good computational performance for the entry vehicle with the guidance cycle update time being 1 s. The terminal time error and the heading error under the double-corridor are shown in Fig. 8. The initial time error is caused by the initial position dispersions and successfully eliminated after few modification cycles of the heading error corridor. Since the aerodynamic dispersions exist, the adjustment of heading error corridor is still conducted during the following flight when the error exceeds the time error corridor boundary.

D. Comparison of Guidance Methods

To verify the advantage of the proposed lateral guidance method, a comparative testing is conducted. The comparison considers three lateral guidance methods as follows:

Method 1: Use a fixed heading error corridor whose boundary is determined in the nominal case.

Method 2: Use an adjustable heading error corridor and an open-loop trajectory predictor for the terminal time.

Method 3 (Proposed method): Use an adjustable heading error corridor and a closed-loop trajectory predictor for the terminal time.

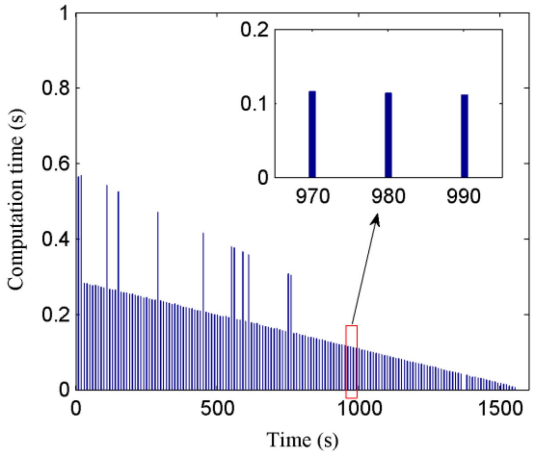

Fig. 7. Computational cost for the proposed guidance method.

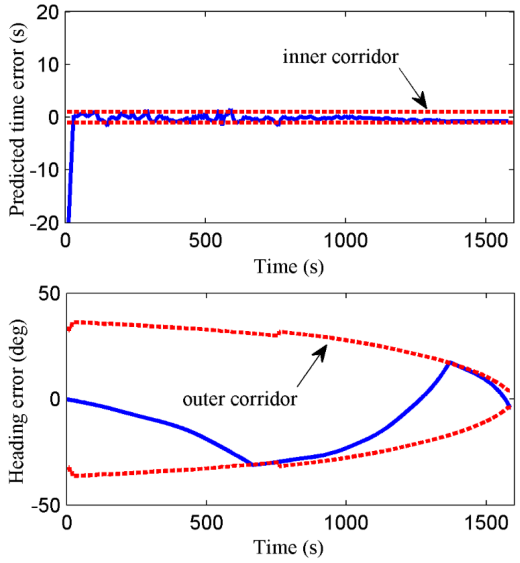

Fig. 8. Terminal time error and heading error under double-corridor.

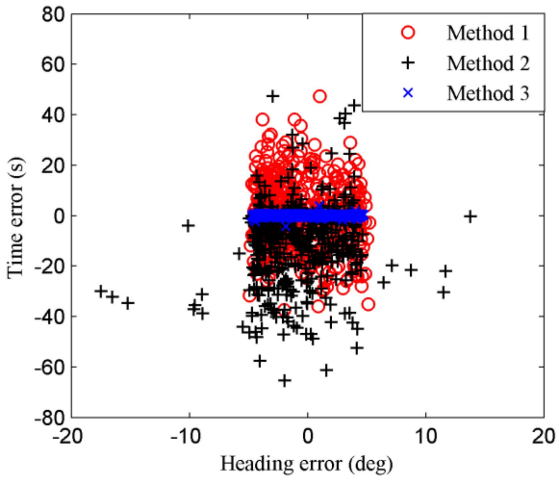

Fig. 9. Terminal time error and heading error in dispersed cases.

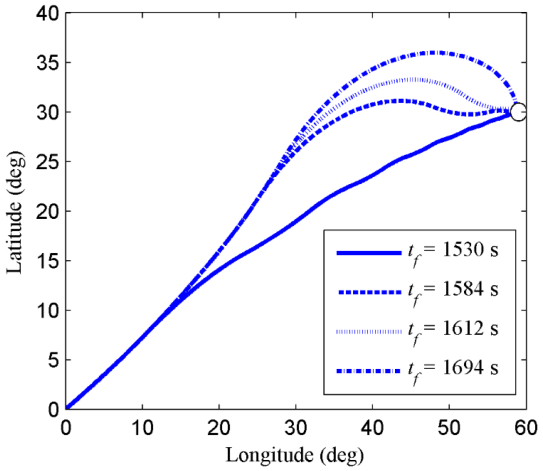

Fig. 10. Ground tracks for various t_f.

Methods 1 and 2 are both verified in the 500 dispersed cases that are used in Section IV-C for Method 3. Errors of the terminal time and the heading angle are shown in Fig. 9. Method 1 using the fixed corridor performs well in controlling the heading error. However, without the corridor modification for the terminal time, the maximum time error is over 40 s. Method 2 can adjust the corridor boundary, but the adjustment is based on an open-loop predictor. As a result, the terminal time error cannot be accurately predicted and eliminated. Moreover, the unreasonable adjustment of the corridor causes large heading errors in some cases. In contrast, the proposed method, i.e., Method 3, is capable of reducing the time error without increasing the heading error. Therefore, the comparison indicates the advantage of the proposed method using the adjustable heading error corridor and the closed-loop trajectory predictor.

E. Variation With Desired Terminal Time

The proposed guidance method is verified for various desired terminal time. In addition to the case of 1584 s, another three cases with the terminal time being 1530 s (the minimum time), 1612 s (average time), and 1694 s (the maximum time) are considered. The ground tracks for the four cases are illustrated in Fig. 10. The vehicle's lateral maneuver is demonstrated to increase with the terminal time. Fig. 11 compares the heading errors and the corridors of the cases. For the smallest terminal time $t_f = 1530$ s, the corridor decreases obviously in the early phase with high velocity. Under the narrow corridor, 14 bank reversals are performed. For $t_f = 1612$ s corresponding to the average feasible time, the corridor is relatively wide and causes only three bank reversals. For $t_f = 1694$ s, which is the maximum feasible time, the widest corridor is used. Although the heading error satisfies the terminal constraint, the corridor hardly works and the heading angle is likely to be out of control when dispersions exist.

Monte Carlo simulations under the same dispersions are conducted for $t_f = 1612$ s, and compared with the results for $t_f = 1584$ s. The accuracy of the terminal altitude and velocity does not vary much for these two cases, because the same longitudinal tracking law is employed. The main difference is the control accuracy of the terminal time.

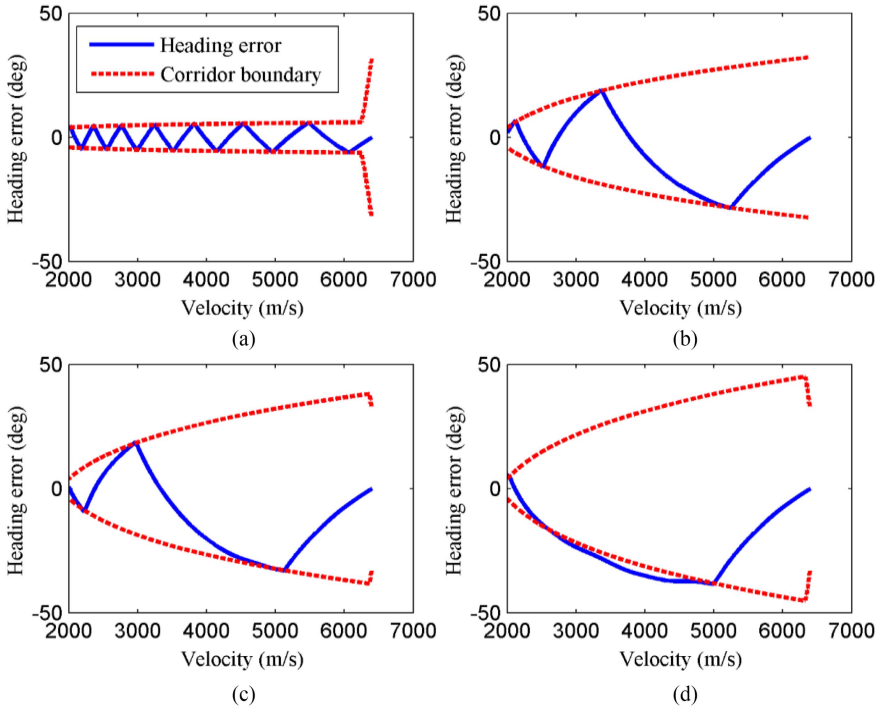

Fig. 11. Heading errors for various t_f. (a) $t_f = 1530$ s. (b) $t_f = 1584$ s. (c) $t_f = 1612$ s. (d) $t_f = 1694$ s.

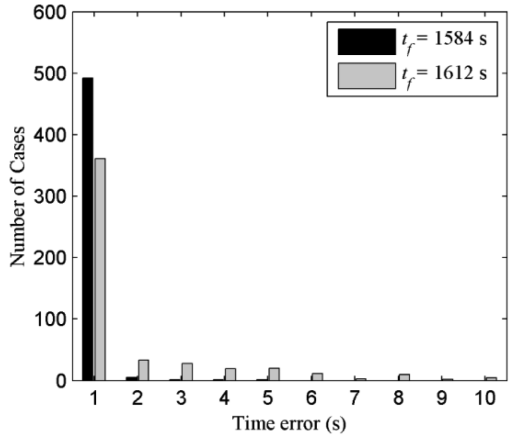

Fig. 12. Terminal time errors for $t_f = 1584$ s and $t_f = 1612$ s in dispersed cases.

The terminal time errors (absolute value) are compared in Fig. 12. The terminal time $t_f = 1584$ s yields a 98.4% rate for the time error lower than 1 s. However, for the terminal time $t_f = 1612$ s, the rate reduces to 76.4%, which indicates the advantage of the desired terminal time given by (32). Consider a larger acceptable time error of 5 s, the rate for $t_f = 1584$ s and $t_f = 1612$ s reaches to 100% and 98.0%, respectively. Apart from the advantage of the desired terminal time, the effectiveness of the proposed lateral guidance logic is demonstrated again.

V. CONCLUSION

To fulfill the requirement of the cooperative gliding flight of multiple entry vehicles, a lateral entry guidance method with the terminal time constraint has been proposed. The guidance method consists of a closed-loop trajectory predictor, a novel lateral guidance logic based on a double-corridor, and a terminal time determination approach based on a feasibility index. The simulation results demonstrate that the lateral guidance logic cooperates well with the longitudinal profile tracking law. A high accuracy is achieved by the terminal time control without reducing the accuracy of the conventional terms (i.e., the terminal altitude, velocity, and heading angle). The computational performance is acceptable because the corridor allows a low modification rate and each modification needs only two predicted trajectories. The variation with the desired terminal time is assessed; the results indicate that the proposed method is applicable to various desired terminal time, and the time given by the feasibility index is more achievable in dispersed cases.

REFERENCES

[1] J. C. Harpold and C. A. Graves, "Shuttle entry guidance," *J. Astronaut. Sci.*, vol. 27, no. 3, pp. 239–268, 1979.
[2] A. Saraf, J. A. Leavitt, D. T. Chen, and K. D. Mease, "Design and evaluation of an acceleration guidance algorithm for entry," *J. Spacecraft Rockets*, vol. 41, no. 6, pp. 986–996, 2004.
[3] S. Li and X. Jiang, "Review and prospect of guidance and control for Mars atmospheric entry," *Prog. Aerosp. Sci.*, vol. 69, pp. 40–57, 2014.
[4] P. Lu, C. W. Brunner, S. J. Stachowiak, G. F. Mendeck, M. A. Tigges, and C. J. Cerimele, "Verification of a fully numerical entry guidance algorithm," *J. Guid. Control, Dyn.*, vol. 40, no. 2, pp. 230–247, 2017.
[5] B. Xu, J. Sun, S. Li, and T. Cao, "Finite time sliding sector control for spacecraft atmospheric entry guidance," *Acta Astronaut.*, vol. 163, pp. 108–113, 2019.

[6] M. Sagliano and E. Mooij, "Optimal drag-energy entry guidance via pseudospectral convex optimization," *Aerosp. Sci. Technol.*, vol. 117, 2021, Art. no. 106946.
[7] W. Huang et al., "Design and realization of recovery system of chang'e-5 reentry spacecraft," *Space Sci. Technol.*, vol. 2021, pp. 1–10, 2021.
[8] T. R. Jorris and R. G. Cobb, "Three-dimensional trajectory optimization satisfying waypoint and no-fly zone constraints," *J. Guid., Control, Dyn.*, vol. 32, no. 2, pp. 551–572, 2009.
[9] Z. Liang, Q. Li, and Z. Ren, "Waypoint constrained guidance for entry vehicles," *Aerosp. Sci. Technol.*, vol. 52, pp. 52–61, 2016.
[10] Z. Liang and Z. Ren, "Tentacle-based guidance for entry flight with no-fly zone constraint," *J. Guid., Control, Dyn.*, vol. 41, no. 4, pp. 991–1000, 2018.
[11] W. Yu et al., "Analytical entry guidance for no-fly-zone avoidance," *Aerosp. Sci. Technol.*, vol. 72, pp. 426–442, 2018.
[12] Z. Liang, J. Yu, Z. Ren, and Q. Li, "Trajectory planning for cooperative flight of two hypersonic entry vehicles," in *Proc. 21st AIAA Int. Sp. Planes Hypersonics Technol. Conf.*, Xiamen, China, 2017, Paper AIAA 2017-2251.
[13] Z. Li, B. He, M. Wang, H. Lin, and X. An, "Time-coordination entry guidance for multi-hypersonic vehicles," *Aerosp. Sci. Technol.*, vol. 89, pp. 123–135, 2019.
[14] Z. Liang, J. Long, S. Zhu, and R. Xu, "Entry guidance with terminal approach angle constraint," *Aerosp. Sci. Technol.*, vol. 102, 2020, Art. no. 105876.
[15] J. Zhao, R. Zhou, and Z. Dong, "Three-dimensional cooperative guidance laws against stationary and maneuvering targets," *Chin. J. Aeronaut.*, vol. 28, no. 4, pp. 1104–1120, 2015.
[16] I.-S. Jeon, J.-I. Lee, and M.-J. Tahk, "Impact-time-control guidance law for anti-ship missiles," *IEEE Trans. Control Syst. Technol.*, vol. 14, no. 2, pp. 260–266, Mar. 2006.
[17] S. He and D. Lin, "Three-dimensional optimal impact time guidance for antiship missiles," *J. Guid., Control, Dyn.*, vol. 42, no. 4, pp. 941–948, 2019.
[18] I.-S. Jeon, J.-I. Lee, and M.-J. Tahk, "Impact-time-control guidance with generalized proportional navigation based on nonlinear formulation," *J. Guid., Control, Dyn.*, vol. 39, no. 8, pp. 1885–1890, 2016.
[19] D. Cho, H. J. Kim, and M.-J. Tahk, "Nonsingular sliding mode guidance for impact time control," *J. Guid., Control, Dyn.*, vol. 39, no. 1, pp. 61–68, 2016.
[20] J. Zhou and J. Yang, "Guidance law design for impact time attack against moving targets," *IEEE Trans. Aerosp. Electron. Syst.*, vol. 54, no. 5, pp. 2580–2589, Oct. 2018.
[21] J. Wang and R. Zhang, "Terminal guidance for a hypersonic vehicle with impact time control," *J. Guid. Control Dyn.*, vol. 41, no. 8, pp. 1790–1798, 2018.
[22] J. Yu, X. Dong, Q. Li, Z. Ren, and J. Lv, "Cooperative guidance strategy for multiple hypersonic gliding vehicles system," *Chin. J. Aeronaut.*, vol. 33, no. 3, pp. 990–1005, 2020.
[23] W. Yu, Y. Yao, and W. Chen, "Analytical cooperative entry guidance for Rendezvous and formation flight," *Acta Astronaut.*, vol. 171, pp. 118–138, 2020.
[24] Y. Guo, X. Li, H. Zhang, L. Wang, and M. Cai, "Entry guidance with terminal time control based on quasi-equilibrium glide condition," *IEEE Trans. Aerosp. Electron. Syst.*, vol. 56, no. 2, pp. 887–896, Apr. 2020.
[25] G. Dukeman, "Profile-following entry guidance using linear quadratic regulator theory," in *Proc. AIAA Guid. Navig. Control. Conf. Exhib.*, Monterey, CA, USA, 2002, Paper AIAA 2002-4457.
[26] A. J. Roenneke and P. J. Cornwell, "Trajectory control for a low-lift re-entry vehicle," *J. Guid., Control, Dyn.*, vol. 16, no. 5, pp. 927–933, 1993.
[27] P. Lu, S. Forbes, and M. Baldwin, "Gliding guidance of high L/D hypersonic vehicles," in *Proc. AIAA Guid., Navig., Control. Conf.*, Boston, MA, USA, 2013, Paper AIAA 2013-4648.
[28] S. Li and X. Jiang, "RBF neural network based second-order sliding mode guidance for Mars entry under uncertainties," *Aerosp. Sci. Technol.*, vol. 43, pp. 226–235, 2015.
[29] Z. Shen and P. Lu, "Dynamic lateral entry guidance logic," *J. Guid., Control, Dyn.*, vol. 27, no. 6, pp. 949–959, 2004.
[30] N. X. Vinh, A. Busemann, and R. D. Culp, *Hypersonic and Planetary Entry Flight Mechanics*. Ann Arbor, MI, USA: Univ. of Michigan Press, 1980.
[31] Z. Shen and P. Lu, "Onboard generation of three-dimensional constrained entry trajectories," *J. Guid., Control, Dyn.*, vol. 26, no. 1, pp. 111–121, 2003.
[32] Z. R. Putnam, M. J. Grant, J. R. Kelly, R. D. Braun, and Z. C. Krevor, "Feasibility of guided entry for a crewed lifting body without angle-of-attack control," *J. Guid., Control, Dyn.*, vol. 37, no. 3, pp. 729–740, 2014.
[33] T. H. Phillips, "A common aero vehicle (CAV) model, description, and employment guide," Schafer Corp. for Air Force Research Laboratory and Air Force Space Command, 2003.
[34] P. Lu, "Predictor-corrector entry guidance for low-lifting vehicles," *J. Guid., Control, Dyn.*, vol. 31, no. 4, pp. 1067–1075, 2008.

Zixuan Liang received the B.E. degree in automation and the Ph.D. degree in guidance navigation and control from Beihang University, Beijing, China, in 2011 and 2016, respectively.

He is currently a Professor with the School of Aerospace Engineering, Beijing Institute of Technology. His research interests include planetary entry guidance, missile guidance, deep space exploration, and flight/orbital control.

Chang Lv received the B.E. degree in automation from Shandong University, Jinan, China, in 2019. He is currently working toward the Ph.D. degree in aeronautical and astronautical science and technology with the Beijing Institute of Technology, Beijing, China.

His research interests include spacecraft trajectory planning and guidance.

Shengying Zhu received the B.S. degree in aerospace engineering and the Ph.D. degree in flight vehicle design from the Harbin Institute of Technology, Harbin, China, in 2004 and 2010, respectively.

He is currently a Professor with the School of Aerospace Engineering, Beijing Institute of Technology, Beijing, China. His research interests include spacecraft system and autonomous technology for deep space exploration.